Journal of Marine Science and Technology

Volume 25 | Issue 6 Article 10

SIMULATION AND MOTION ANALYSIS OF DEEPWATER MANIFOLD LIFTING

Zhiwei Chen
School of Reliability and Systems Engineering at Beihang University, Beijing, China.

Tingdi Zhao
School of Reliability and Systems Engineering at Beihang University, Beijing, China.

Jian Jiao
School of Reliability and Systems Engineering at Beihang University, Beijing, China., jiaojian@buaa.edu.cn

Dongfeng Mao
Offshore Oil and Gas Research Center, China University of Petroleum (Beijing), Beijing, China.

Journal of Marine Science and Technology, Vol. 25, No. 6, pp. 696-704 (2017)
DOI: 10.6119/JMST-017-1226-10

SIMULATION AND MOTION ANALYSIS OF DEEPWATER MANIFOLD LIFTING

Zhiwei Chen[1], Tingdi Zhao[1], Jian Jiao[1], and Dongfeng Mao[2]

Key words: lifting installation method, manifold, motion response, time domain.

ABSTRACT

The development and utilization of oil and gas resources has expanded to deep water. The installation of a subsea manifold is crucial for developing offshore oil-gas fields. In this study, we used the lifting installation method (LIM) to install a subsea manifold. First, the appropriate environmental parameters were selected through the analysis of environmental loads at the Liwan 3-1 Gasfield in the South China Sea. The wind and wave spectra were selected using noise power density and Joint North Sea Wave Project spectra, respectively. The entire lifting and installation system that responds to environmental loads comprised a vessel, cable, and manifold. The time history of motion response was obtained through simulation and time-domain analysis for the entire lifting and installation process under the combined effect of wind, waves, and current. The motion response of the manifold and the cable tension were analyzed in three stages (entering, steady lowering, and landing phases). The results indicate that the motion responses of the vessel and manifold were highest in the direction of the environmental load. Moreover, the results indicated that the tension of the cable was highest during the entering phase. Furthermore, a heave compensation mechanism was used to reduce the vertical motion of the subsea manifold and the cable tension during the lifting process, which facilitated correct decision-making and reduced the risk of an accident.

I. INTRODUCTION

With an increasing demand for oil and gas resources, the oil and gas development and exploration industry is gradually focusing on the ocean, particularly the deep sea (Stock et al., 2002). Currently, the depth of development in the West African sea has exceeded 1000 m and the drilling depth has exceeded 2000 m, whereas the depth of development in Brazil has been ≥ 3000 m (Liu et al., 2006). The construction of marine structures entails high levels of input, technology, and risk. The deepwater manifold is a high cost, large volume, and internally complex structure. Therefore, lowering and installing the manifold to the seabed is particularly essential. During offshore installation, the entire operating system, including the installation vessel and manifold, is influenced by the environmental load, such as that caused by wind, waves, and current. Errors in the lifting and installation process incur substantial risks and losses under poor operating conditions.

The following installation methods of deepwater manifolds have been extensively studied: the drilling riser installation method (DRIM), lifting installation method (LIM), sheave installation method, pendulous installation method (PIM), pencil buoy method, and wet tow installation method (Zhang and Xie, 2011; Wang et al., 2012).

The LIM is the primary technique for installing manifolds in deep water, and this technique involves two main methods (Cermelli et al., 2003):

(1) Transportation of the manifold to the installation site using a vessel and then the lowering of the manifold to the installation position using the cable of a crane or winch;
(2) Transfer of the manifold onto a mobile drilling ship and then lowering of the manifold to the installation position using a drilling riser.

The installation depth for the LIM is approximately 1500 m due to the limitations of vessels and installation equipment. The average depth of the Liwan 3-1 Gasfield is approximately 1500 m (Cao et al., 2012). To lower the manifold in the Liwan 3-1 Gasfield, multifunctional engineering vessel 286, built by the CNOOC and able to operate at a water depth of 3000 m, was employed. This vessel met the requirements of the LIM.

The entire dynamic system, which responded to environmental loads such as wind, waves, and current in a complex manner, was composed of a vessel, winch, cable, and manifold. The deepwater installation technology has the following three primary aspects: lifting/lowering technology, dynamic response to environmental loads, and positioning and control techniques (Wang et al., 2017). Therefore, for lifting and installing the entire mani-

Paper submitted 09/14/17; revised 10/18/17; accepted 11/15/17. Author for correspondence: Jian Jiao (e-mail: jiaojian@buaa.edu.cn).
[1] School of Reliability and Systems Engineering at Beihang University, Beijing, China.
[2] Offshore Oil and Gas Research Center, China University of Petroleum (Beijing), Beijing, China.

fold, the dynamic response and environmental loads cannot be neglected. Wu et al. (2016) established the mathematical model of underwater load lifting by considering the effects of various factors, such as ocean environment, lifting depth, mass, added mass coefficient, and the damping coefficient of the system. Hong et al. (2016) proposed an equation for the motion of a multibody system, where the crane boom was considered deformed due to the deadweight and weight of the suspenders. Bi et al. (2013) presented a mathematical model of a subsea cable laying system and studied the system's dynamic properties through numerical simulation. Richter et al. (2016) developed a nonlinear discrete model of a lifting system by considering the nonlinear drag forces, structural rope damping, and snap loads through time-domain simulations. Li et al. (2014) simulated the processes of a manifold entering the water and the underwater pendulous motion of the manifold using nonlinear time-domain coupled analysis. Wang et al. (2013) analyzed the entire installation of a manifold by using the PIM and then compared its effective cost with those of the LIM and DRIM. Nam et al. (2016) conducted an experiment of deepwater lifting and lowering operations of a subsea manifold by considering the effects of wave conditions, water depth, and equipment weight. Bai et al. (2014) presented a 3D mechanical analysis method of manifold installation by considering the response amplitude operator, waves, and lowering velocity. Jiang et al. (2013) established a mechanical model of the DRIM and LIM and consequently validated the model by comparing its results with those of finite element analysis. Jeong et al. (2016) analyzed the wire tension and collision detection of an offshore support vessel and equipment by calculating dynamic responses. Nam et al. (2013) investigated the effects of passive and active heave compensators (AHCs) on deepwater lifting operation through a nonlinear time-domain analysis. Choi et al. (2016) investigated AHC performance during deepwater installation through experiments and numerical simulation.

In this study, we analyzed the marine environment conditions during lifting and installation of a deepwater manifold. To install the manifold at a depth of 1500 m in the Liwan 3-1 Gasfield, suitable wave, wind, and current spectra were selected according to different wave, wind, and flow theories. The vessel, cable, winch and manifold comprise the entire lifting and installation system which is responding to environmental loading due to wind, waves and current in a complex way. During the installation of the equipment (multifunctional offshore vessel 286 and Dyneema cable), the lifting of the manifold was investigated using the LIM. Numerical simulation and coupled response analysis were performed for the entire installation process. Considering the combined effects of wind, waves, and current, the numerical simulation process was as follows. First, the static offset of the vessel and manifold was obtained through static analysis of the entire lifting process. The six degrees of freedom (SDOF) motion of the vessel and the motion response of the manifold was then analyzed through the dynamic analysis of the whole LIM in the time domain. The results of the static and dynamic analyses of the manifold displacement offset were compared. Finally, the entire lifting process was divided into three typical phases: the entering, steady lowering, and landing phases. The time history of the displacement, velocity, and acceleration of the manifold and the cable tension were analyzed by coupling the time-domain analyses in different stages.

The rest of the paper is organized as follows. The environmental load analysis and parameter selection are presented in Section II. Section III describes the entire lifting and installation system including the manifold, installation cable, and engineering vessel. The coupled response analysis of the lifting process and time-domain analysis of the three stages are described in Section IV, and conclusions are provided in Section V.

II. DESCRIPTION OF ENVIRONMENTAL LOADS

1. Environmental Loads

Environmental loads are caused by environmental phenomena (Veritas, 2000). The environmental phenomena related to ocean engineering structures can damage such structures, disturb their operation, or cause navigation failures (Veritas, 2000). According to the environment of the Liwan 3-1 Gasfield, this study focused on the following offshore structure phenomena: wind, waves, and current. Parameters were selected based on DNV-RP-H103 as follows: sea water temperature, density, and kinematic viscosity were 15°C, 1025.9 kg/m^3, and 1.19×10^6 m^2/s, respectively; air density and movement viscosity were 1.226 kg/m^3 and 1.45×10^{-5} m^2/s, respectively.

2. Wind Loads

Wind speed varies with time and height above the ground or sea surface (Veritas, 2000). Ocean engineering structures are superstructures with a large wind-affected area and wind sensitivity. Wind induces a mean healing moment for fixed structures and a mooring force for floating structures. Considering the time variation in wind forces, a dynamic wind analysis is necessary for the analysis of wind-exposed equipment, and such analysis may be sensitive to varying wind loads. Low-frequency resonant surge, sway, and yaw motion of floating catenary anchored platforms can be induced using the time-varying component of the wind force (Veritas, 2000). According to the American Petroleum Institute (API) RP2SK 2005, the wind spectra of the API and noise power density (NPD) are widely applied in marine engineering. The NPD spectrum was used for modeling the Liwan 3-1 Gasfield. The wind direction, surface friction coefficient, and surface wind speed were 180°, 0.2, and 12.9 m/s, respectively.

The instantaneous wind force on the wind-exposed structure was calculated by summarizing the instantaneous force and each wind-exposed member. The instantaneous wind pressure q can be calculated using the following formula (Veritas, 2000):

$$q = \frac{1}{2}\rho_a \left|U(t,z)+u-\dot{x}\right|\left(U(t,z)+u-\dot{x}\right) \tag{1}$$

where ρ_a is the mass density of dry air, u is the gust speed and direction variation, and $U(t, z)$ and $\dot{x}$ are the mean wind speed and instantaneous velocity of the structural member, respectively.

If the wind power spectrum density $S(f)$ is known, the gust speed and direction variation is given as follows:

$$u = \sqrt{2S(f)\Delta f} \ . \tag{2}$$

The force F_w acting on a structure or surface and perpendicular to the structure axis or surface is given by:

$$F_w = CqA \cdot \sin(\alpha) \tag{3}$$

where C and A are the effective shape factor and cross-sectional area of the wind load surface, respectively. α represents the angle between the wind direction and load surface.

3. Wave Loads

Oceanic engineering structures are affected by waves in constantly changing sea conditions. The shape, length, height, and speed of propagation of ocean waves are irregular and random. Wave loads consist of drag force, inertial force, and diffraction force. According to the DNV specification, a 3-parameter JONSWAP spectrum was selected through a random spectral method for irregular waves. The peak (γ), significant wave height, and wave period were 1, 1.5 m, and 9.8 s, respectively, and the direction was 180°. According to a calculation using Morison formula, wave loads are widely enforced in small scale offshore structures.

The drag coefficient (C_d) and added mass coefficient (inertial force coefficient, C_m) in the Morison formula cannot be determined directly on the basis of the theory. Through numerous theoretical and experimental studies conducted over decades, researchers have obtained the law of variation of C_d and C_m, which includes the Reynolds number, Keulegan-Carpenter number, and roughness. Morison et al. (1995) proposed that the wave force (f) acting on a cylinder per unit length is determined by

$$f = \frac{1}{2} C_d \rho D \left| u \right| u + \frac{\pi}{4} C_m \rho D^2 \frac{\partial u}{\partial t} \tag{4}$$

where D and ρ are the diameter and mass density of the fluid, respectively.

The velocity and acceleration of the water particles can be determined using wave theory. Therefore, the selected coefficient should be consistent with wave theory. For structures of a general shape, extensive tests and analyses must be conducted to determine C_d and C_m. Various ship classification societies and relevant departments have made recommendations regarding the selection of C_d and C_m values, as shown in Table 1.

4. Current Loads

The total current velocity included the wind-generated, tidal, and water wave velocities. A steady current acting on offshore structures was simplified into linear variations. The surface and current velocities were 1.30 and 0.09 m/s, respectively, at 300 m above the sea level. The current velocity was constant at 0.09 m/s below 300 m in the direction of the wind and waves. The distribution of tidal current velocity is related to the vertical distance from the still water level z, which may be given by a simple power law (Veritas, 2000) as follows:

$$u_t(z) = (1 + \frac{z}{d})^{\frac{1}{7}} u_t(0) \tag{5}$$

where $u_t(0)$ is the tidal current velocity at z and d is the water depth from z (taken positive).

The wind-generated current can be expressed in a linear form as follows:

$$u_w(z) = (1 + \frac{z}{d}) u_w(0) \tag{6}$$

where $u_w(0)$ is the tidal current velocity at z.

Upon considering the water wave velocity u_{wave}, the total current velocity $u(z)$ is as follows:

$$u(z) = u_t(z) + u_w(z) + u_{wave} \ . \tag{7}$$

Table 1. Values of C_d and C_m adopted by national norms.

National norms	China	API standard of the USA	Norway marine Inspection Bureau
Wave theory	Linear	Stokes fifth-order	Stokes fifth-order
C_d	1.2	0.6-1.0	0.5-1.2
C_m	2.0	1.5-2.0	2.0

Table 2. Main parameters of the manifold.

Description	Value
Weight (t)	195
Water depth (m)	1500
Volume (m)	(13.50,5.2,4.5)
Center of gravity	(-0.05,0.11,1.43)

III. DESCRIPTION OF THE ENTIRE SYSTEM

1. Deepwater Manifold

To simplify the modeling and hydrodynamic calculation, upon ensuring that the projection area of each direction was unchanged, the model was reduced to a cuboid as shown in Fig. 1. The main parameters of the manifold are displayed in Table 2.

To analyze the manifold condition, the resistance caused by waves in deepwater was not considered. Generally, when a manifold is lowered into water, it is subjected to frictional resistance

Table 3. Main parameters of the installation cable.

Description	Value
Breaking strength (t)	1000
Diameter (mm)	170
Length(m)	2000
Weight in air (kg/m)	21.0
Weight in water (kg/m)	7.40
Safety factor	4

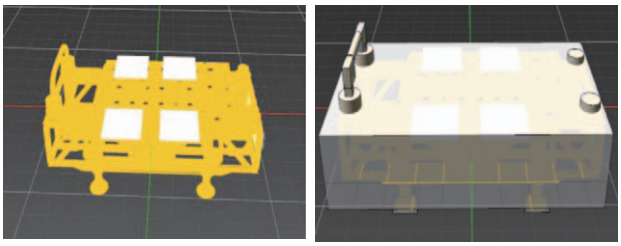

Fig. 1. Simplified manifold model.

and pressure drag. The total resistance F_D is the sum of frictional resistance and pressure drag (Veritas, 2000):

$$F_D = C_D A_D \rho u_0^2 / 2 \tag{8}$$

where C_D is the drag coefficient, A_D is projected area of the manifold in the direction of incoming flow, and u_0 is the relative velocity between the manifold and the water.

Moreover, the unsteady motion of the manifold under water produces an added mass force (F_{add}). F_{add} cannot be neglected unless the acceleration is extremely small. The relationship between the added mass force and added mass is as follows:

$$F_{add} = m_{ij}\alpha \tag{9}$$

where m_{ij} is the added mass and α is the relative acceleration between the manifold and the water.

Due to environmental factors such as wind, waves, and current, the manifold may experience heaving, flip, torsion, and other movements. In particular, when the manifold is substantially heavy and thus has large inertia, control of the manifold is easily lost, which causes severe losses. The following two important factors should be considered during the manifold installation process.

1) Carrying Capacity of a Cable

The safe working load of a cable is the sum of the actual load and cable weight. Considering the cable carrying capacity provides a basis for the safety of the cables.

2) Dynamic Response

During deepwater manifold installation, the hull experiences a heaving motion on the sea surface. This motion is transferred to the manifold by the cable. The dynamic response produces additional dynamic tension loads in the cable (Stock et al., 2002).

Table 4. Main parameters of the vessel 286.

Description	Value
LOA (m)	140.75
LBP (m)	127.85
BEAM (m)	29.00
Scantling Draught (m)	9.00
Mass (t)	14150
LCG (m)	64.22 (From AP)
TCG (m)	-0.10 (From centerline)
VCG (m)	11.37 (From baseline)

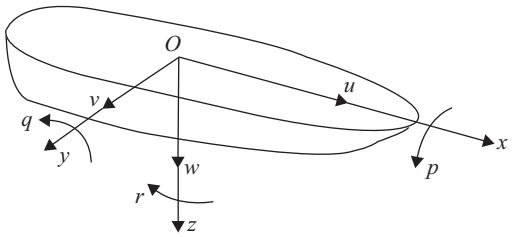

Fig. 2. Six degrees of freedom of vessel motion.

2. Installation Cable

The length of the installation cable was approximately 2000 m. A Dyneema cable was used to lower and install the manifold (Zhu, 1986). Two cables were required to meet the ultimate load requirements and ensure the safety of the entire installation process. The main parameters of the cable are shown in Table 3.

3. Engineering Vessel

A ship is typically considered a rigid body with SDOF, as illustrated in Fig. 2. The rectilinear motions along the three axes—*u, v,* and *w*—are surge, sway, and heave, respectively. The rotational motions around the three axes—*p, q,* and *r*—are roll, pitching, and yaw, respectively. The ship considered in this study was a multifunctional offshore vessel 286 built by CNOOC. The speed of the ship was 11 knots, with the maximum operating water depth 3000 m. The dynamic positioning system DP3 was used. The main parameters of the vessel are shown in Table 4.

IV. NUMERICAL SIMULATION AND CALCULATION ANALYSIS

The lifting and installation system comprised a vessel, cable, winch, and manifold. The system responded to environmental loading, such as wind, waves, and current, in a complex manner. Numerical simulation and coupled response analysis were performed for the entire installation process.

To obtain stationary statistics, time-domain analysis of the structural response due to random load effects must be strictly

Table 5. Parameters of winch speed and time.

Start time (s)	Stop time (s)	Speed (m/s)	Lowering distance
0.00	200.0	0.2	40
200.0	1200.0	0.05	50
1200.0	8200.0	0.2	1400
8200.0	9200.0	0.05	50

Table 6. Results of static calculation.

Position (m)	X		Y		Z	
	Initial	Offset	Initial	Offset	Initial	Offset
Vessel	-80.2	0.00	0.00	0.00	-0.0952	-0.093
Manifold	-76.1	-2.2	83.3	3.0	46.9	-0.38
Angle (°)	R_X		R_Y		R_Z	
	Initial	Offset	Initial	Offset	Initial	Offset
Vessel	-0.378	-0.38	-0.0234	-0.023	0.00	0.00
Manifold	-0.810	1.7	-2.14	0.36	0.119	0.12

conducted (Veritas, 2000). Therefore, to identify the risk and ensure the operational reliability of the installation process, the combined effects of various factors-including velocity, acceleration, and tension-were calculated.

The dynamic installation process was analyzed in the time domain. First, the time history of motion was obtained for the entire lifting process of the manifold. The motion response of the vessel, tension response of the cable, and displacement and velocity were then calculated under typical conditions.

The winch was controlled using preset control. The lowering process, lasting 9200 s, was divided into three stages: the entering, steady lowering, and landing phases. The entire process of entering the water was composed of two parts: pre-entering and entering. The winch parameters of the vessel are shown in Table 5. Initially, the manifold was 47.3 m above the sea surface and was then lowered by 40 m. The speed of the manifold was 0.2 m/s before it was immersed in water. The speed then decreased to 0.05 m/s, and the manifold was lowered by 50 m. The manifold was then completely in the water, and lowering was performed smoothly at a speed of 0.2 m/s; the speed decreased to 0.05 m/s once the manifold had been lowered by 50 m. Subsequently, once the manifold had been lowered to 50 m from the seabed, the winch speed was decreased to 0.05 m/s and the manifold was gradually lowered to the seabed.

1. Overall Analysis of the System

1) Static Analysis

A static analysis of the entire process was conducted. The initial position and angle and static analysis result of the vessel and manifold are shown in Table 6.

The position of the vessel exhibited a minor change, and the vessel experienced a slight heaving motion; the offset was -0.093 m. Small deflection angles of -0.38° and -0.023° along the X and Y axes, respectively, were observed. These deflection angles indicate that the ship was stationary during the static analysis, without any large swings or rotations. However, the offset of the manifold was greater than that of the vessel. The motion response of the manifold was higher due to environmental load and ship motion, but was nonetheless under control.

2) Dynamic Analysis

The time history of the SDOF motion of the offshore vessel is presented in Fig. 3. The vessel experienced a low-frequency motion response in the form of sway, surge, and yaw and a high-frequency motion response in the form of heave, roll, and pitch. The average surge distance was -0.02 m, and the range of motion of the surge, from -78.5 m to -85.3 m, was larger than those of the sway and heave. The pitch angle from 0.6° to -0.62° was larger than those of the roll and yaw. These differences were due to the effects of wind, waves, and current in the X direction (corresponding to 180°). The azimuth of the vessel was along the direction of the environmental forces, which effectively reduced the influence of the ship's motion response on the manifold. The amplitude of manifold movement in the X direction ranged between -65 m and -86 m. The rotation around the X-axis ranged from 0.1° to - 1.6°. The amplitude reached a maximum when the manifold became immersed in water (1200 s). The results reveal that the manifold produced a greater torque and rotational motion because of the influence of the environmental loads. Controlling the lowering speed and time is necessary to avoid a large rotation angle.

The static and dynamic analyses of the manifold displacement offset are compared in Table 7. The manifold exhibited a larger motion response and fluctuation range in the X direction than in the other directions. It was susceptible to environmental forces and vessel motion, causing an increase in response and offset.

2. Entering Phase

The entire process of entering the water within 1200 s was

Table 7. Static and dynamic analysis of manifold displacement.

Analysis	Offset of *X*/m	Offset of *Y*/m
Static	-2.2	3.0
Dynamic	8.9~-12.1	5.1~1.2

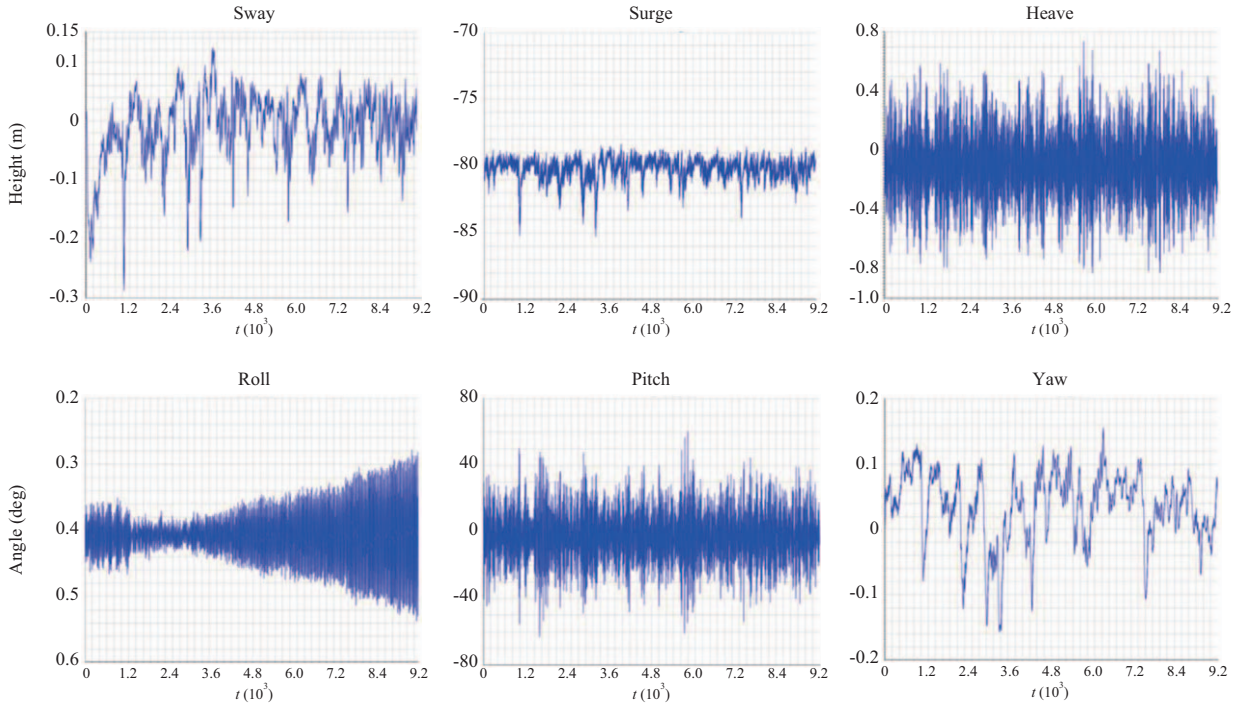

Fig. 3. Motion time history of the vessel in the entre lowering phase.

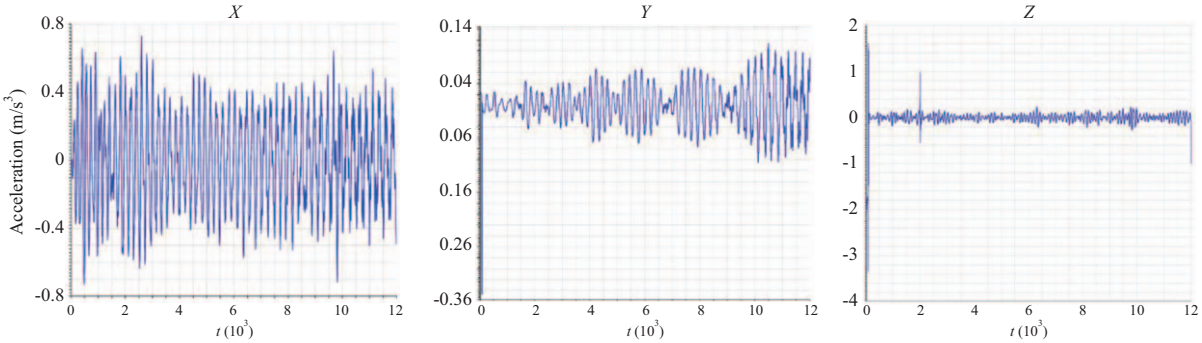

Fig. 4. Acceleration time history of the manifold in the entering phase.

composed of two parts: pre-entering and entering. Initially, the manifold was positioned 47.3 m above the sea surface and was subsequently lowered by 40 m. The speed of the manifold was 0.2 m/s before it touched the water. Thereafter, the speed was decreased to 0.05 m/s, and the manifold was lowered by 50 m.

The time history of the time-domain analysis during the entering phase is shown in Fig. 4. The acceleration in the *X* direction of the manifold was larger, which indicates that the manifold had poor stability during the entering stage. The winch had to be slowed before the manifold entered the water to prevent increases in the relative manifold velocity and avoid an accident. The cable tension changed considerably. The average tension was 125 t, and the maximum tension was 217 t, as shown in Fig. 5. The breaking strength of the cable was 1000 t, and the safety factor was 4. Therefore, the maximum tension was less than the maximum permissible tension (250 t), and thus the tension caused

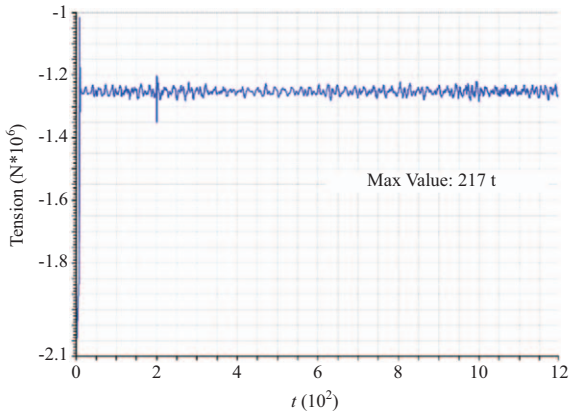

Fig. 5. Tension time history of the cable in the entering phase.

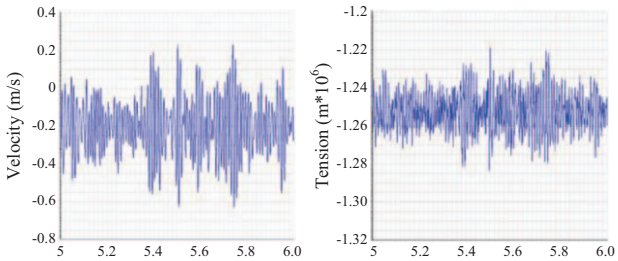

Fig. 6. Time history for the *Z* direction in the steady lowering phase.

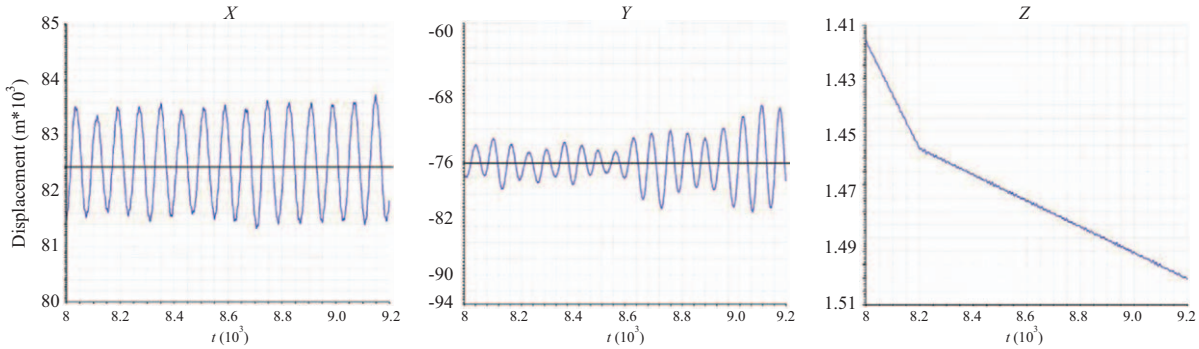

Fig. 7. Displacement time history of manifold in the landing phase.

by acceleration did not break the cable.

3. Steady Lowering Phase

During the entire process of steady lowering within 6000 s, the manifold was completely immersed in water and lowered smoothly at a speed of 0.2 m/s. The manifold was lowered by 900-1000 m within approximately 5000-6000 s. A cable's flexibility and resilience increases with increasing cable length; thus, the fluctuation amplitude of the manifold increased. The operation was relatively smooth, and the cable did not break. This result demonstrated that the entire process was relatively stable, with no obvious change in the velocity of the manifold and tension of the cable in the *Z* direction. The time history for the *Z* direction in the steady lowering phase is presented in Fig. 6.

4. Landing Phase

The entire landing phase lasted approximately 1000 s. The winch began to decelerate when the manifold was 50 m above the seabed, and the speed was decreased to 0.05 m/s. The manifold was then gradually lowered to the seabed. The displacement time history of the manifold in the landing phase is shown in Fig. 7. The deviations of the manifold in the *X* and *Y* directions were -2.24 m and 3.21 m, which coincided with the static calculation results. Small fluctuations occurred in the location of the manifold due to the influence of vessel motion response in the *Z* direction. As illustrated in Fig. 8, the average heave velocity of the vessel was 0.00007 m/s and that of the manifold was 0.168 m/s. These velocities indicates that the vertical mo-

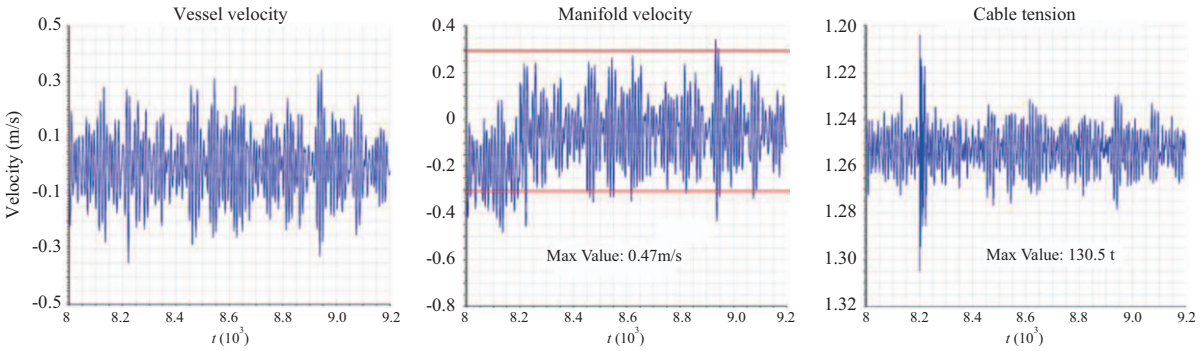

Fig. 8. Time history for the *Z* direction in the entering phase.

tion response of the manifold was stronger because of the effects of the wind, waves, current, and vessel heave. The maximum fluctuant velocity of the manifold in the *Z* direction reached 0.47 m/s, which was greater than the safe lowering speed (0.3 m/s). Therefore, the manifold fluctuation should be prevented from becoming too large and the manifold should be prevented from colliding with other seabed structures. An AHC mechanism was used to reduce the vertical displacement of the manifold. When the speed of the winch was decreased to 0.05 m/s, the cable tension changed suddenly. The maximum tension reached 130.5 t, which was within the permissible tension range. Overall, the deviation of the manifold in the landing phase could be controlled. In the LIM, controlling the manifold can reduce location errors and meet the accuracy requirement. Therefore, using the LIM to lower a manifold under the selected experimental conditions is safe and feasible.

V. CONCLUSION

In this paper, according to the actual operational conditions of the Liwan 3-1 Gasfield in the South China Sea and the actual installation cable and vessel, the entire manifold lifting process and coupled response of the manifold are discussed. Based on the results of the analysis, the following observations were made:

(1) The motion responses of the vessel and manifold were largest in the direction of the environmental load. To avoid excessive deviation of the manifold, the dynamic positioning of the vessel in the load direction should be strengthened. During the manifold lifting process, the azimuth of the vessel can be aligned along the environmental direction, which can reduce the influence of vessel motion response on the manifold.
(2) The cable tension was highest during the entering phase. Deceleration of the winch caused the maximum tension in the cable before the manifold was immersed in water. The maximum tension of 217 t was less than the permissible tension of 250 t; thus, the tension caused by the deceleration did not break the cable.
(3) At different depths, the vertical motion trajectories of the vessel and manifold exhibited small fluctuations, with the vertical fluctuation amplitude of the manifold larger than that of the vessel. During the manifold lifting process, the highest fluctuant velocity of the manifold in the *Z* direction was 0.47 m/s, which was higher than the safe speed. A heave compensation mechanism should be used to reduce the vertical motion of the subsea manifold and the cable tension to prevent the collision of the manifold with other seabed structures.

This paper identifies many promising directions that can be taken in future studies. The maximum tension could be analyzed in the future by considering the influence of bending and torsion on permissible tension.

REFERENCES

Bai, Y., W. Ruan, S. Yuan, X. He and J. Fu (2014). 3D mechanical analysis of subsea manifold installation by drill pipe in deep water. Ships and Offshore Structures 9(3), 333-343.

Bi, G., S. Zhu, J. Liu, X. Fang and L. Wang (2013). Dynamic simulation and tension compensation research on subsea umbilical cable laying system. Journal of Marine Science and Application 12(4), 452-458.

Cao, S. R., J. X. Yu, G. Z. Zhang and W. L. Ma (2012). A Study on the Controllability of Deepwater Manifold during Launch through Pendulous Installation Method. In Advanced Materials Research (Vol. 490, pp. 1992-1996). Trans Tech Publications.

Cermelli, C., D. Morrison, H. C. San Martin and M. Guinn (2003). Progression of ultradeep subsea deployment systems. In Offshore Technology Conference. Offshore Technology Conference.

Choi, Y. M., B. W. Nam, S. Y. Hong and J. W. Kim (2016). An Experimental Study on the Subsea Structure Installation using the Active Heave Compensator. In The 26th International Ocean and Polar Engineering Conference. International Society of Offshore and Polar Engineers.

Hong, J. W., M. I. Roh, S. H. Ham and S. Ha (2016). Dynamic simulation of subsea equipment installation using an offshore support vessel based on flexible multibody system dynamics. Journal of Marine Science and Technology 24(4), 807-821.

Jeong, D. H., M. I. Roh and S. H. Ham (2016). Lifting simulation of an offshore supply vessel considering various operating conditions. Advances in Mechanical Engineering 8(6), 1687814016654633.

Jiang, H., W.-D. Ruan, H. D. Qiao, W. J. Qian and Y. Bai (2013). Mechanical analysis of subsea manifold lowered into deep water. Ship Engineering.

Liu, J.-m., S.-S. Wang, F. Wei, X. Yu and W. Lu (2006). The discusses of deepwater oilfield development engineering options and its adaptability in the South China Sea. China Offshore Oil and Gas 18(6), 413-418.

Li, X., J.-X. Yu, Q.-J. Zhou, W.-L. Ma and H.-J. Yin (2014). Numerical simu-

lation of the installation of deepwater manifold through pendulous installation method. Journal of Ship Mechanics 18(9), 1072-1085.

Morison, J. R., J. W. Johnson and S. A. Schaaf (1950). The force exerted by surface waves on piles. Journal of Petroleum Technology 2(05), 149-154.

Nam, B. W., Hong, S. Y., Kim, Y. S. and Kim, J. W. (2013). Effects of passive and active heave compensators on deepwater lifting operation. International Journal of Offshore and Polar Engineering, 23(01).

Nam, B. W., N. W. Kim, Y. M. Choi and S. Y. Hong (2016). A Model Test for Deepwater Lifting and Lowering Operations of a Subsea Manifold. International Journal of Offshore and Polar Engineering 26(03), 263-271.

Richter, M., F. Zeil, D. Walser, K. Schneider and O. Sawodny (2016). Modeling offshore ropes for deepwater lifting applications. In Advanced Intelligent Mechatronics (AIM), 2016 IEEE International Conference on (pp. 1222-1227). IEEE.

Stock, P. F., M. B. de Cerqueira and F. E. Roveri (2002). A new method for deploying subsea hardware in deep water. Proceedings of the 2002 Deep Offshore Technology, New Orleans, USA.

Veritas, N. (2000). Environmental conditions and environmental loads. Det Norske Veritas.

Wang, A., Y. Yang, S. Zhu, H. Li, J. Xu, and M. He (2012). Latest progress in deepwater installation technologies. In: Proceedings of the 22nd ISOPE International Offshore and Polar Engineering Conference, 17-22 June, Rhodes, Greece

Wang, A. M., S. Zhu, X. Zhu, J. Xu, M. He and C. Zhang (2013). Pendulous installation method and its installation analysis for a deepwater manifold in South China Sea. In The Twenty-third International Offshore and Polar Engineering Conference. International Society of Offshore and Polar Engineers.

Wang, Y., M. Duan, H. Liu, R. Tian and C. Peng (2017). Advances in deepwater structure installation technologies. Underwater Technology 34(2), 83-91.

Wu, Y., J. Lu and C. Zhang (2016). Study on dynamic characteristics of coupled model for deep-water lifting system. Journal of Ocean University of China 15(5), 809-814.

Zhang, J. and Y. Xie (2011). Research and development of subsea manifold installation methods. Ocean Engineering (Haiyang Gongcheng) 29(1), 143-148.

Zhu, D. (1986). Force in the hoisting wire between a crane barge and a floating heavy. Ocean Engineering 4(1).